Korean J. Chem. Eng., **30**(6), 1187-1194 (2013)
DOI: 10.1007/s11814-013-0042-7

Modelling and analysis of pre-combustion CO_2 capture with membranes

Ji Hye Choi*, Myung-June Park*,†, JeongNam Kim, Youngdeok Ko**, See-Hoon Lee***, and Ilhyun Baek****

*Department of Chemical Engineering, Ajou University, Suwon 443-749, Korea
**Greenhouse Gas Center, Korea Institute of Energy Research (KIER), Daejeon 305-343, Korea
***Department of Resources and Energy Engineering, Chonbuk National University, Jeonbuk 561-756, Korea
(*Received 7 November 2012 • accepted 19 March 2013*)

Abstract−A pre-combustion CO_2 capture system was modelled with three different membranes. It comprised an amine absorber for the elimination of H_2S, high- and low-temperature water gas shift reactors for the conversion of CO to CO_2 and a membrane to keep over 90% of the CO_2 in the retentate. The absorber and equilibrium reactors were modelled using rigorous models, while the partial least squares model was used for three different types of membranes to predict the experimental results. The effectiveness of the modelling of the reactors and membranes was tested through comparison of simulated results with experimental data. The effects of operating pressure and membrane type are also discussed, and it was found that using a smaller membrane under high pressure lowered the membrane's cost but also lowered energy recovery.

Key words: Pre-combustion, CO_2 Capture, Membrane, Modelling, Partial Least Squares (PLS) Model

INTRODUCTION

Carbon capture and storage (CCS) is essential to reducing CO_2 emissions, with there being several types, including post-combustion, pre-combustion and oxyfuel combustion. Post combustion capture involves CO_2 being captured from flue gas by scrubbing with a recoverable amine solvent. Oxy combustion uses oxygen for combustion instead of air, producing flue gas mainly comprising CO_2 and H_2O. Pre-combustion capture is used in gas turbine combined cycles [1], and despite its name does not capture CO_2 before combustion.

Absorption processes are commonly used, with chemical absorption using monoethanolamine (MEA) an important CO_2 capture method for treating power plants' flue gases [2]. However, much work has focused on pre-combustion capture, which possesses important advantages. Franz and Scherer [3] reported pre-combustion capture in coal fired power plants and focused on the application of polymeric membranes for gas separation. Pre-combustion CO_2 capture is often via an integrated gasification combined cycle (IGCC), since current atmospheric pressure post-combustion absorbers require higher capital costs, and the cost of replacing degraded solvent makes pre-combustion capture favorable for producing low-carbon electricity [4]. Pre-combustion capture requires smaller equipment than post-combustion capture since it employs high CO_2 concentrations and pressures, and different solvents can be used with low energy penalties for regeneration [5]. Its main disadvantage is the very high total capital costs of the generating facility.

Since its introduction in the 1980s, membrane separation has been used both in the petrochemical industry and in the cleaning of natural gas before transport. Polymer membranes have been commercially successful in comparison with absorption processes or cryogenic fractionation [6]. Membranes have great potential applicability for both CO_2 and H_2 separation in gasification processes for various reasons, including that the removal of gas through selective film ensures high energy efficiency, low-volume equipment and low capital costs compared with conventional separation processes [7-9]. Scholes et al. [9] reported technical and design issues of the inclusion of membrane gas separation in pre-combustion carbon capture as part of an IGCC.

However, there are few quantitative cost analyses of pre-combustion CO_2 capture. Therefore, we applied conceptual modelling to evaluate the effects of operation pressure and membrane type on energy efficiency to find the best configuration and conditions for pre-combustion CO_2 capture. An empirical PLS model is presented for different membranes, with rigorous models being used for the absorber, and equilibrium models being used for the reactors.

MATERIALS AND METHODS

Simulated gas, comprising CO, H_2 and CO_2 in a 65/30/5 ratio, was used to evaluate the performance of the WGS reactor. Catalysts for the high-temperature (HTS) and low-temperature (LTS) water gas shift reactors were from Süd-Chemie Catalysts Japan Inc. The composition for HTS catalyst (product name: SHT-4) was 86-92 wt% iron oxide, 6-10 wt% chromium oxide, 0.1-2.0 wt% chromium trioxide and 1.5-2.1 wt% copper oxide. The LTS catalyst (product name: MDC-7) consisted of 40-44 wt% copper oxide, 44-50 wt% zinc oxide and 7.0-13 wt% aluminum oxide. After the pressure stabilized, heaters in each unit operation were manipulated until the specified temperatures were reached (steam heater: 250 °C, pre-heater: 400 °C, HTS heater: 380 °C, LTS heater: 220 °C). After reaching steady pressure and temperature, an HPLC pump was used to provide water, and the generation of steam was confirmed in a by-pass

†To whom correspondence should be addressed.
E-mail: mjpark@ajou.ac.kr

line. Finally, the nitrogen gas was replaced by the simulated gas and the reactor effluents were analyzed by gas chromatography (GC).

As the reactor stabilized, the temperature of the membrane was also stabilized by flowing hydrogen gas at 20 bar. The Pd-Cu membrane developed by the Korea Institute of Energy Research (KIER) was set at 400 °C, and the commercial membranes were operated at 300 °C, as recommended by their manufacturer (Nalson Co. Ltd., Japan). The thicknesses of KIER and commercial membranes were 4 and 20 μm, respectively; their areas, 16.6 and 70 (500) cm^2, respectively. Both types of membrane had 40% copper compositions. The effluent from the membrane was analyzed by GC and a non-dispersive infra-red (NDIR) analyzer.

RESULTS AND DISCUSSION

1. Pre-combustion CO_2 Capture System under Reference Conditions

Fig. 1 outlines the pre-combustion CO_2 capture system with the incorporated membrane considered herein. Streams were labelled by the unit operations from which they originated. For example, the stream labelled "COOLER_output" represents the exit stream from the COOLER operation. UniSim Design Suite (Honeywell Inc.) was used for the simulations; detailed information on the streams is listed in Table 1. Mole fractions were calculated excluding water from the stream because the changes of CO, CO_2 and H_2 fractions

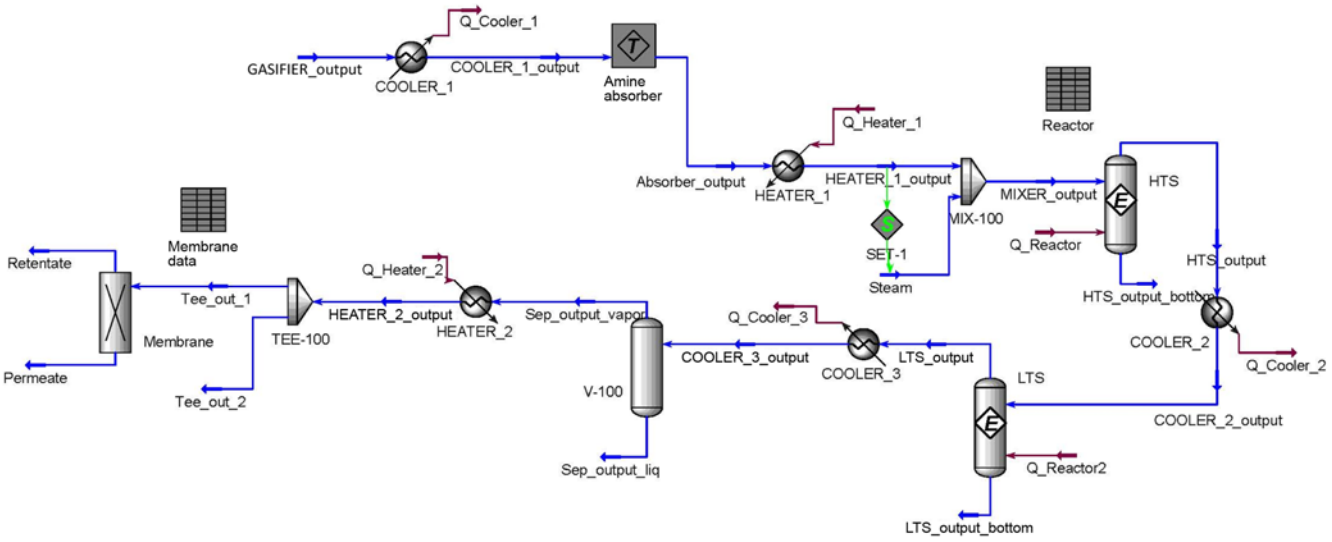

Fig. 1. A pre-combustion CO_2 capture system with membrane.

Table 1. The main streams of pre-combustion CO_2 capture with the 70 cm^2 membrane

Stream name	Vapour fraction	Temperature [°C]	Pressure [kPa]	Molar flow [kgmol/h]	Mole fraction[a]					
					CO	H_2	CO_2	N_2	H_2S	MDEA
GASIFIER_output	1	**1400**	**3000**	4.09	**0.65**	**0.3**	**0.03**	**0.02**	**0**	**0**
COOLER_output	1	**200**	3000	4.09	0.65	0.3	0.03	0.02	0	0
HE_1_output	1	**40**	3000	4.09	0.65	0.3	0.03	0.02	0	0
Absorber_output	1	55.13	3000	4.01	0.66	0.3	0.02	0.02	0	0
HE_2_output	1	**380**	3000	4.01	0.66	0.3	0.02	0.02	0	0
Steam	1	384	3000	10.62	0	0	0	0	0	0
MIXER_output	1	**380**	3000	4.01	0.66	0.3	0.02	0.02	0	0
HTS_output	1	380	3000	6.58	0.01	0.58	0.4	0.01	0	0
HE_3_output	0.99	**200**	3000	6.58	0.01	0.58	0.4	0.01	0	0
LTS_output	1	**200**	3000	6.66	0	0.58	0.41	0.01	0	0
HE_4_output	0.46	**60**	3000	6.66	0	0.58	0.41	0.01	0	0
Sep_output_vapor	1	60	3000	6.63	0	0.58	0.4	0.01	0	0
Sep_output_liq	0	60	3000	7.96	3.43e-5	1.75e-2	0.98	1.05e-3	3.47e-5	2.56e-5
HE_5_output	1	**300**	3000	6.63	0	0.58	0.4	0.01	0	0
Tee_out_1	1	300	3000	1.01e-2	0	0.58	0.4	0.01	0	0
Tee_out_2	1	300	3000	5.19	1.11e-3	0.58	0.40	1.21e-2	4.13e-6	1.11e-7
Permeate	1	304.1775	100	5.73e-3	0	1	0	0	0	0
Retentate	1	300	3000	4.41e-3	0	0.04	0.93	0.03	0	0

[a]Mole fraction of the dry gas; Water is excluded in the calculation of mole fraction

through the units are the major concern of this work. Bold type numbers denote specified values; other values were calculated by the process simulator.

The feed stream ("GASIFIER_output") is comprised of syngas (CO and H_2), CO_2 and N_2. The total flow of 100 Nm^3/hr and its composition (Table 1) are based on the coal gasifier operating at 1 ton per day (TPD). *Ca.* 1,000 ppm hydrogen sulfide (H_2S) is included in the feed stream and an amine-based absorber should be considered for its removal to prevent poisoning of the catalysts in the water-gas-shift (WGS) reactors. In the reference case, the pressure is maintained at 30 bar throughout the process units. The effects of operating pressure are discussed later.

Temperature changes along the unit operations are shown in Fig. 2. Temperature abruptly decreases at the amine absorber and increases prior to the high temperature WGS reactor (HTS). In the case of exothermic reaction, equilibrium conversion is inverse to temperature, and thus, the LTS reactor has higher equilibrium conversion than HTS reactor. However, the HTS reactor is introduced prior to the LTS reactor because of the faster reaction rates at its higher temperature. This allows the reactors to occupy less volume than if only an LTS reactor was used.

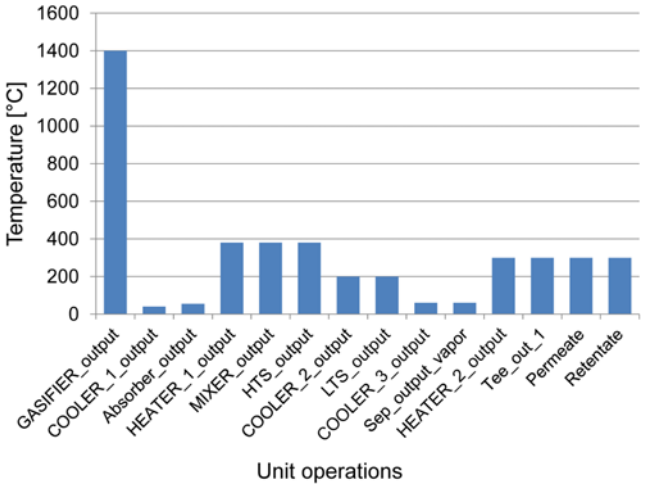

Fig. 2. Temperature changes along the unit operations of the pre-combustion CO_2 capture system.

An amine absorber was designed using a sub-template (the "Amine Absorber" in Fig. 1). Details of the process, composed of an absorber and a stripper, are provided in Fig. 3. The absorber was specified to reduce the amount of H_2S from 1,000 ppm to 10 ppm, using methyl diethanolamine (MDEA) absorbent. Other specifications are listed in Table 2.

To maximize CO conversion, excess water was fed into the WGS reactor (steam to CO ratio=4). Since an HTS reactor usually operates at 350-400 °C, a 380 °C feed temperature was specified here. The

Table 2. Absorber specification

		Specification	
		Absorber	Stripper
Trays			7
Solvent		MDEA	Water
Temperature [°C]	Feed	40	120
	Top	55.13	41.77
	Bottom	56.25	121.47
Pressure [kPa]	Feed	3000	670.11
	Top	3000	189
	Bottom	3000	203

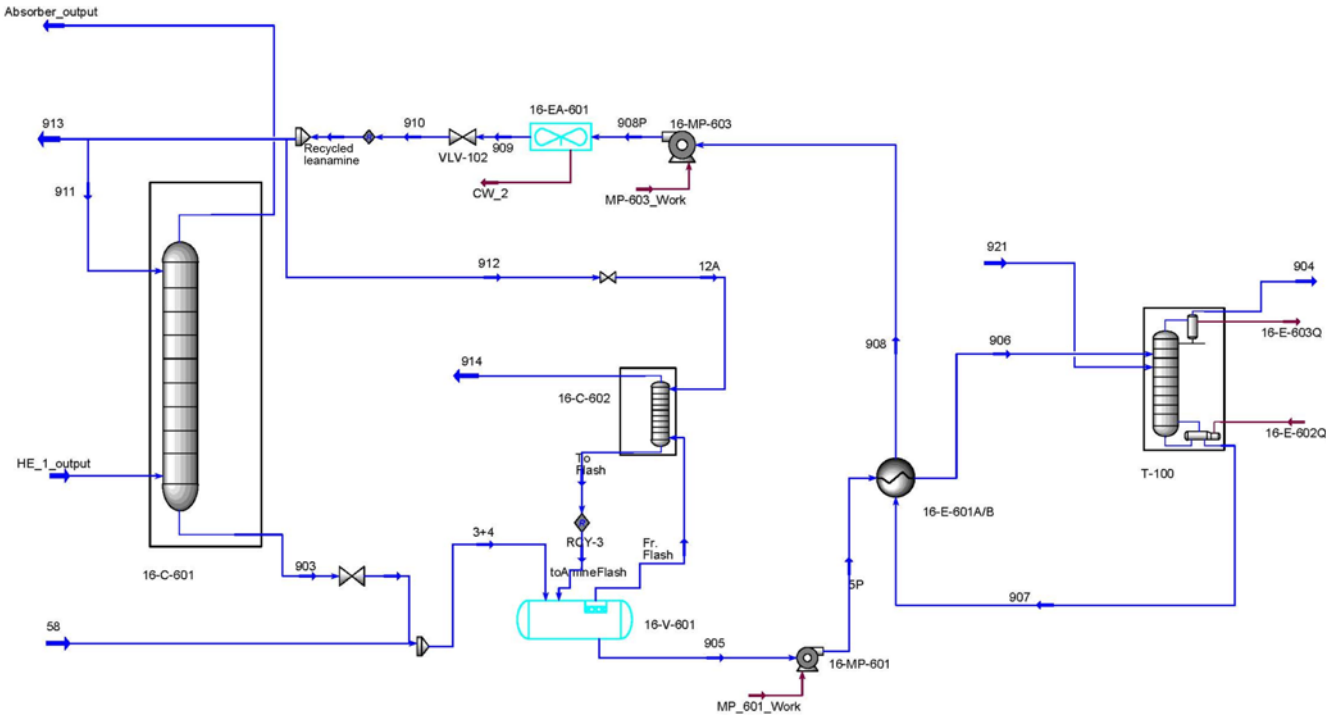

Fig. 3. An amine absorber.

LST reactor was operated at 200 °C. Local conversions in the HTS and LTS reactors (conversions on the basis of feed conditions of each reactor) were calculated to be 96.64% and 91.98%, respectively. The global conversion was 99.73%. 98.78% conversion was observed experimentally, demonstrating the satisfactory performance of the model. It is worth noting that the equilibrium of both HTS and LTS reactors was guaranteed by loading more amount of catalysts than required for the reaction to reach the equilibrium. Therefore, an equilibrium reactor was used for the simulation, and the model showed less than 1% of error compared to the experimental data.

Water in the LTS reactor's effluent can deteriorate the separation performance of the membrane and so should be eliminated by a flash operation (V-100 in Fig. 1). Most of the water liquefied at 60 °C and 30 bar, decreasing its presence from 54.6 mol% to 8.30×10^{-3} mol%.

2. Partial Least Squares Membrane Modelling

Multiple linear regression (MLR) is a general method of constructing models Y=f(X) [10]. It can be represented mathematically as:

$$Y=XB+E_{MLR} \tag{1}$$

where **X**, **Y**, **B** and $\mathbf{E}_{MLR}$ represent the regressor (or input) block, the response (or output) block, the regression (or sensitivity) matrix and the residual matrix, respectively. When the number of independent variables (m) is lower than the number of samples (n), there is no exact solution but an approximate solution can be determined by minimizing the magnitude of the residual vector ($\mathbf{E}_{MLR}$). The least squares solution is given by:

$$\mathbf{B}=(\mathbf{X}^T\mathbf{X})^{-1}\mathbf{X}^T\mathbf{Y} \tag{2}$$

This equation reveals a common problem in MLR, namely, the inverse of $\mathbf{X}^T\mathbf{X}$ may be difficult to compute if the input data block is of high dimension and its elements are highly correlated, i.e., showing collinearity or singularity. The partial least squares (PLS) approach is an alternative that can overcome this problem.

PLS methods involve approximating the **X** and **Y** spaces with their respective score matrices and maximizing the correlation between the original data blocks [10,11]. A simplified model involves regression between the scores for the **X** and **Y** blocks. The PLS model can be interpreted as consisting of outer relations (of the **X** and **Y** blocks individually) and an inner relation (linking both blocks). The outer relations for the **X** and **Y** blocks are:

$$X=TP^T+E=\sum_{h=1}^{a}t_hp_h^T+E \tag{3}$$

$$Y=UQ^T+F^*=\sum_{h=1}^{a}u_hq_h^T+F^* \tag{4}$$

Each pair of latent variables accounts for a certain amount of the variability in the input and output blocks. The first a latent variables account for most of the variance of the data blocks and the other latent variables capture measurement and/or process noise in the data. Accurate description of **Y** (make $\|\mathbf{F}^*\|$) and the simultaneous construction of efficient representation between **X** and **Y** are the objects of this model. A simple criterion for model building is to use a threshold value for **F***, but cross validation can be used to determine the number of latent variables for a robust model [12].

The simplest model for the inner relation is the linear:

$$\hat{u}_h=b_ht_h \tag{5}$$

where $b_h=\hat{u}_ht_h/t_h^Tt_h$ is the regression coefficient in the multiple linear regression (MLR) and the principal component regression (PCR) models. The model for predicting output variables is constructed

Table 3. PLS modelling coefficients for each membrane[a]

Size	Input / Output	$x_{1,scaled}$	$x_{2,scaled}$	$x_{3,scaled}$	$(x_{1,scaled})^2$	$(x_{2,scaled})^2$	$(x_{3,scaled})^2$	$x_{1,scaled}x_{2,scaled}$	$x_{1,scaled}x_{3,scaled}$	$x_{2,scaled}x_{3,scaled}$
16.6 cm^2	$y_{1,scaled}$	0.0038	0.3545		0.0038	0.3487		0.2897		
	$y_{2,scaled}$	0.0038	0.3545		0.0038	0.3487		0.2897		
	$y_{3,scaled}$	−0.1731	0.4151		−0.1731	0.4078		0.2809		
	$y_{4,scaled}$	−0.0562	0.3855		−0.0562	0.3791		0.2953		
	$y_{5,scaled}$	0.3922	−0.4272		0.3922	−0.4188		−0.2185		
70 cm^2	$y_{1,scaled}$	0.0036	0.2066	0.1235	0.0011	0.2030	0.1234	0.1849	0.1343	0.1951
	$y_{2,scaled}$	−0.0004	0.2024	0.1287	−0.0030	0.1993	0.1285	0.1794	0.1381	0.1962
	$y_{3,scaled}$	−0.1087	0.3451	−0.0215	−0.1080	0.3088	−0.0200	0.2719	−0.0800	0.1689
	$y_{4,scaled}$	0.0044	0.3424	−0.2227	0.0060	0.2949	−0.2193	0.3174	−0.2463	0.0369
	$y_{5,scaled}$	0.1807	−0.2095	−0.1371	0.1804	−0.1938	−0.1365	−0.1179	−0.0610	−0.1988
500 cm^2	$y_{1,scaled}$	0.0406	0.3081		−0.2328	−0.8761		1.4394		
	$y_{2,scaled}$	0.0406	0.3081		−0.2328	−0.8761		1.4394		
	$y_{3,scaled}$	−0.1052	0.3078		0.0380	0.9499		−0.3510		
	$y_{4,scaled}$	−0.0584	0.3448		−0.0678	0.3195		0.3366		
	$y_{5,scaled}$	0.3083	−0.1410		0.0942	−1.0824		0.8717		

[a]Subscript i of x_i: 1=pressure, 2=feed, 3=H_2/CO_2 ratio; subscript i of y_i: 1=flux, 2=flowrate of H_2 in the permeate, 3 & 4=flowrates of H_2 and CO_2 in the retentate, respectively, 5=fraction of CO_2 in the retentate. Subscript 'scaled' denotes the variables were scaled as $x_{i,scaled}=(x_i-m_i)/\sigma_i$, where m_i and σ_i represent mean and standard deviation of data, respectively (cf. Table 6)

Table 4. Scaling factors of means and standard deviations for PLS modelling

Size	Symbols	Pressure [bar]	Feed [sccm]	H_2/CO_2	Flux [cm^3/(cm^2·min)]	Permeance [cm^3/(cm^2·min)]	H_2 (permeate) [sccm]	H_2 (retentate) [sccm]	CO_2 (retentate) [sccm]	CO_2 fraction (retentate) [%]
16.6 cm^2	m_i	16.67	2.20E+03		60.80		1.00E+03	166.31	1.03E+03	87.94
	σ_i	5.16	1.19E+03		29.69		492.82	152.69	564.06	4.97
70 cm^2	m_i	8.90	2.55E+02	2.38	16.71		1.14E+03	600.88	803.43	61.91
	σ_i	2.02	1.36E+03	1.30	8.81		621.64	517.07	439.96	13.64
500 cm^2	m_i	14.23	1.13E+04		6.46		3.23E+03	3.55E+03	4.52E+03	58.95
	σ_i	4.00	7.35E+03		3.59		1.80E+03	3.14E+03	2.94E+03	6.78

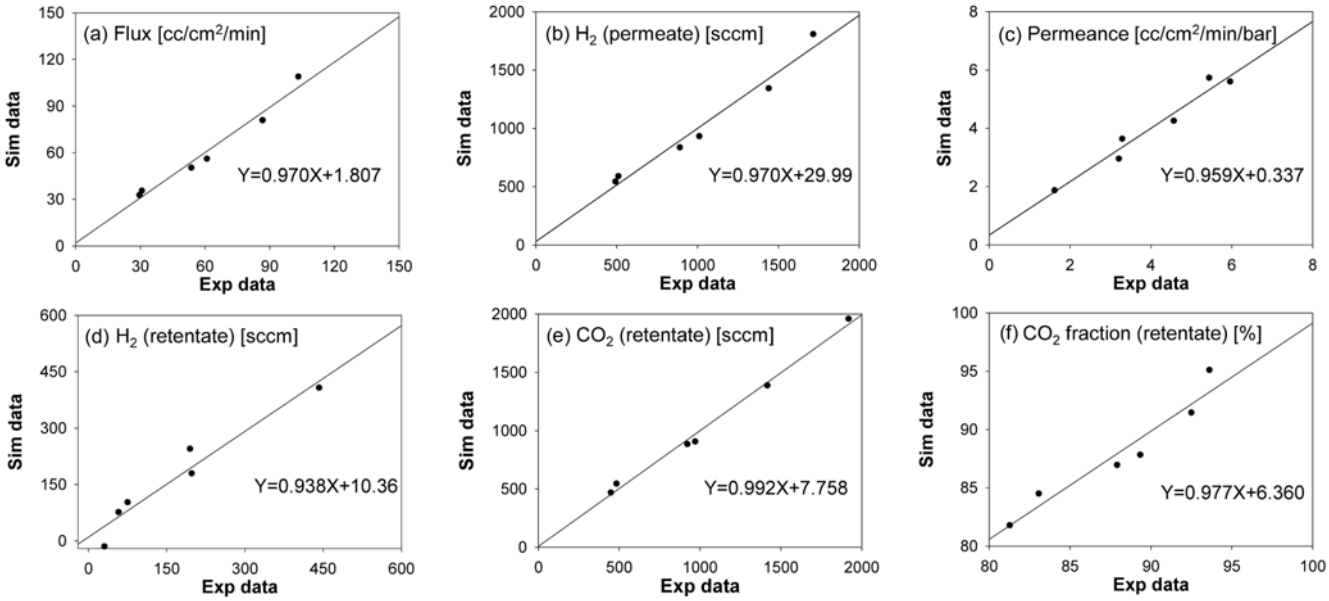

Fig. 4. Parity plots of (a) Flux [cc/cm^2/min], (b) H_2 in permeate [sccm], (c) Permeance [cc/cm^2/min/bar], (d) H_2 in retentate [sccm], (e) CO_2 in retentate [sccm], and (f) CO_2 fraction in retentate for the 16.6 cm^2 membrane.

applying the PLS algorithm in linear regression form as follows [13]:

$$\hat{y}_h = x^T \hat{b} \quad (6)$$

Three different membranes are considered here, with areas of 16.6 cm^2, 70 cm^2 (reference), and 500 cm^2. The reference membrane had pressure (x_1), feed flow rate (x_2) and H_2/CO_2 ratio (x_3) included in the input data block (**X**); they were varied between 6 and 12 bar, 750 and 6,000 sccm and 1 and 4, respectively to obtain 29 experimental data. The H_2/CO_2 ratio was fixed at 1.5 for both the other two membranes; the numbers of experimental conditions were 6 and 13, respectively. Squared terms and cross-products were included in the input vector to address the nonlinearity of the relationship. The output data block (**Y**) included five properties: flux in cc/cm^2/min (y_1), flow rate of H_2 in the permeate (y_2), flow rates of H_2 (y_3) and CO_2 (y_4) in the retentate and the fraction of CO_2 (y_5) in the retentate.

The input and output data blocks were scaled to prevent ill-conditioning problems resulting from the variables' different orders of magnitude; all the variables were scaled to have zero means and unity variances. Two latent variables were required to cover more than 98% and 95% variances of the input and output blocks, respectively, when considering the smallest membrane. The other membranes each required three. The resulting relationships between the input and output blocks are listed in Table 3, the scaling factors in Table 4. Figs. 4-6 compare the experimental and simulated results and clearly demonstrate the satisfactory performance of the PLS-based model.

3. Effects of Operating Pressures

Under reference condition, pressure was assumed to be maintained at 30 bar throughout the entire operation. However, operation at high pressure can adversely affect a reactor and create large pressure differences between the absorber and stripper, increasing energy consumption. To assess the effects of operating pressures on energy efficiency, simulations were conducted at 10, 20 and 30 bar. Energy recovery was calculated by subtracting the energy required for heating from the heat produced by the units (Fig. 7). Much heat was released from the coolers and the HTS reactor. The large difference in the energy required by the smallest membrane and the others (*cf.* HEATER_2 (16.6) and HEATER_2 (70 & 500) in Fig. 7(a)) was attributable to their different operating temperatures (400 °C for 16.6 cm^2 vs. 300 °C for 70 and 500 cm^2), while pressure was shown to have little effect. As a result, energy recoveries

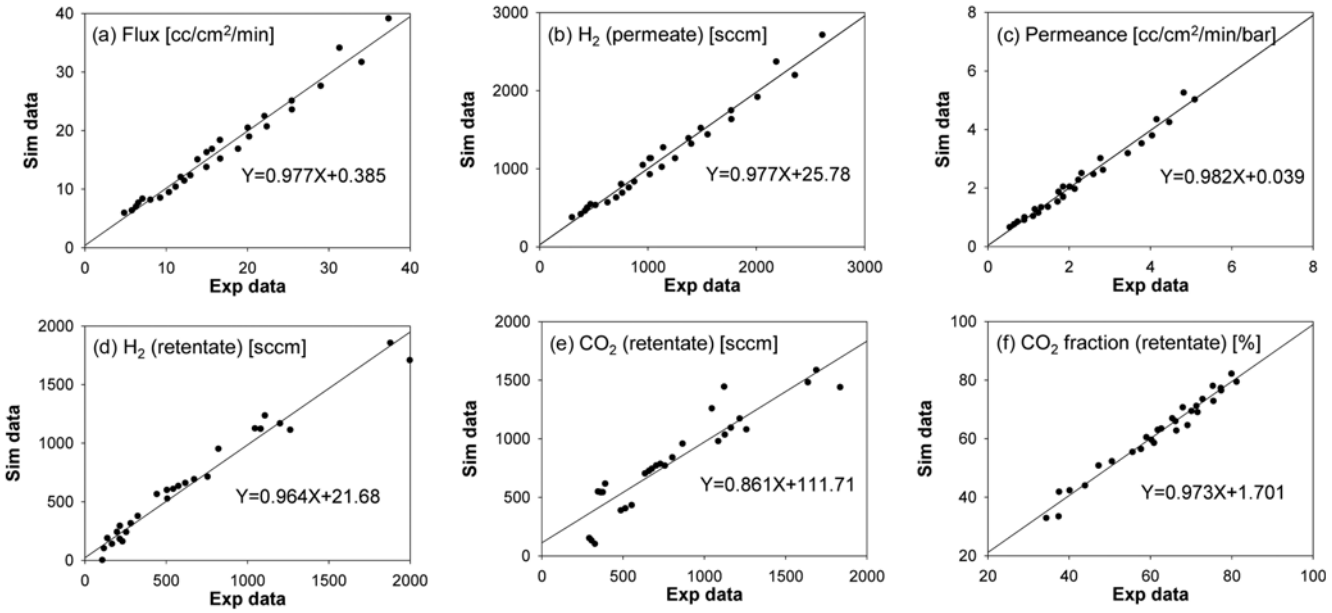

Fig. 5. Parity plots of (a) Flux [cc/cm^2/min], (b) H_2 in permeate [sccm], (c) Permeance [cc/cm^2/min/bar], (d) H_2 in retentate [sccm], (e) CO_2 in retentate [sccm], and (f) CO_2 fraction in retentate for the 70 cm^2 membrane.

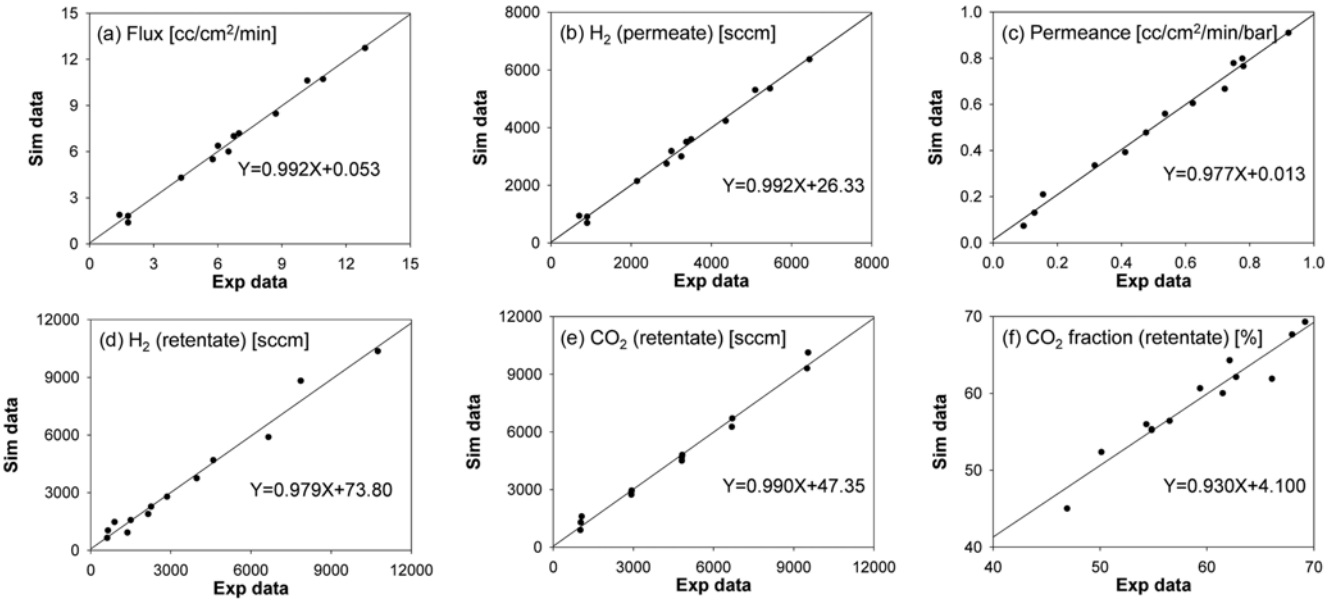

Fig. 6. Parity plots of (a) Flux [cc/cm^2/min], (b) H_2 in permeate [sccm], (c) Permeance [cc/cm^2/min/bar], (d) H_2 in retentate [sccm], (e) CO_2 in retentate [sccm], and (f) CO_2 fraction in retentate for the 500 cm^2 membrane.

using the reference and largest membranes were higher than when using the smallest membrane due to their lower operating temperature. Operation at low and high pressures (10 and 30 bar) released more heat than the energy requirement.

Pressure also affects the number of membranes. Using the model in Table 3, the feed flow rate required to keep 90% of the CO_2 in the retentate was calculated under the corresponding conditions. The total number of each membrane was then calculated by dividing the total flow rate by the calculated feed flow rate. The number of membranes was then multiplied by the unit price (Table 5) to give the total membrane cost for each membrane under each operating pressure (Fig. 8). For the largest membrane, no flow rate could satisfy the condition at 10 and 20 bar. Since increased pressure could enhance the membranes' separation performance, higher pressures led to fewer membranes of any type being required. The smallest membrane showed the lowest membrane cost. It is worth noting that the use of small membranes to satisfy the required CO_2 fraction in the retentate may limit the application of membrane separation to the process with extremely large capacity. However, given the efficiency of the membranes, the process in the present study may be comparable to other CO_2 capture process.

The above discussion shows that high pressure is preferred for

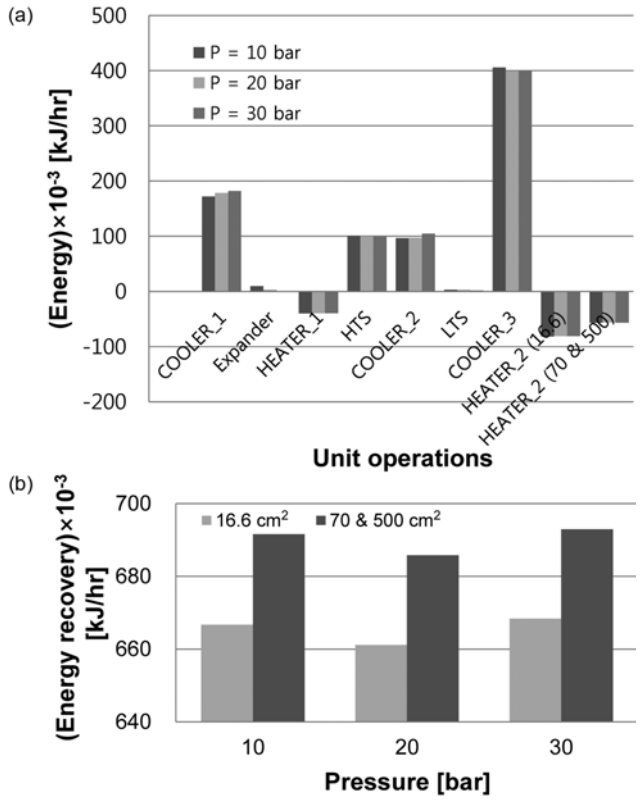

Fig. 7. Plots of (a) energy required and heat produced [kJ/hr] along the unit operations; (b) energy recovery [kJ/hr] under each pressure.

Table 5. Numbers of each membrane under the specified pressures for 90% of CO_2 in the retentate

Size	Pressure [bar]	Numbers	Unit price [KRW/unit]
16.6 cm^2	10	1,169	585,008
	20	2,053	
	30	20,798	
70 cm^2	10	655	5,824,476
	20	1,025	
	30	3,006	
500 cm^2	10[a]	-	17,620,713
	20[a]	-	
	30	227	

[a]The condition of 90% of CO_2 in the retentate could not be satisfied at these pressures

better energy recovery and membrane cost and that smaller membranes lowered capital costs at the expense of operating costs. Since this work considered only energy recovery, which partially includes whole operating expenses, further study may be required to estimate operating costs more accurately under a variety of conditions. In addition, instead of heat exchangers (HX), heaters and coolers were considered here for simplicity, indicating that additional optimization is required to maximize the energy efficiency of an HX network (HEN). Another factor to be considered is the feed composition of the reactor. An H_2O/CO ratio of 4 was assumed for the

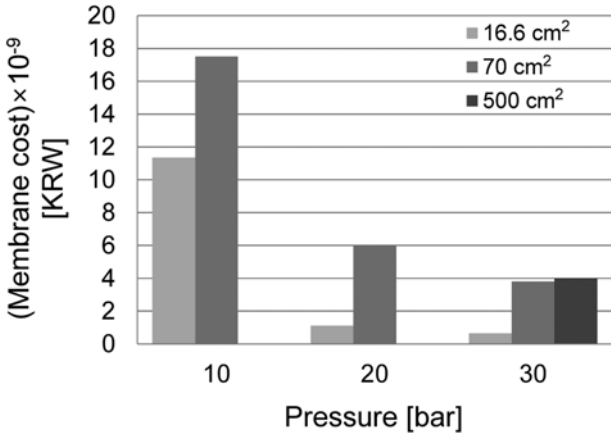

Fig. 8. Membranes' costs under various operating pressures.

complete conversion of carbon monoxide, but too much steam may greatly increase the expense of removing water before the membranes. However, this work clearly shows that the optimal operating pressure and the size of the membranes should be considered, since they significantly affect the capital and operating costs of pre-combustion CO_2 capture.

CONCLUSIONS

The entirety of a pre-combustion CO_2 capture process was modelled by combining rigorous modelling with an empirical partial least squares model. Operating pressure was shown to affect the process's energy efficiency and the manufacturing cost of the membranes. The smallest membrane considered (16.6 cm^2) was the least expensive, and high-pressure operation decreased the number of membranes required. However, it showed worse energy recovery, i.e., efficiency. Overall this modelling approach was shown to be suitable for assessing the optimal configuration and operating conditions of the considered system.

ACKNOWLEDGEMENTS

This work was supported by the Energy Efficiency & Resources Programs of the Korea Institute of Energy Technology Evaluation and Planning (KETEP) grant funded by the Korea government Ministry of Knowledge Economy (No. 20122010200071).

REFERENCES

1. J. Davison, *Energy*, **32**, 1163 (2007).
2. H. J. Herzog, *Environ. Sci. Techonol.*, **35**, 148 (2001).
3. J. Franz and V. Scherer, *J. Membr. Sci.*, **359**, 173 (2010).
4. J. Gibbins and H. Chalmers, *Energy Policy*, **36**, 4317 (2008).
5. A. A. Olajire, *Energy*, **35**, 2610 (2010).
6. W. J. Koros and G. K. Fleming, *J. Membr. Sci.*, **83**, 1 (1993).
7. M. Bracht, P. T. Alderliesten, R. Kloster, R. Pruschek, G. Haupt, E. Xue, J. R. H. Ross, M. K. Koukou and N. Papayannakos, *Energy Convers. Mange.*, **38**, S159 (1997).
8. S. Shelly, *Chem. Eng. Prog.*, **105**, 42 (2009).
9. C. A. Scholes, K. H. Smith, S. E. Kentish and G. W. Stevens, *Int. J.*

Greenh. Gas Con., **4**, 739 (2010).
10. P. Geladi and B. R. Kowalski, *Anal. Chim. Acta*, **185**, 1 (1986).
11. M. A. Sharaf, D. L. Illman and B. R. Kowalski, *Chemometrics*, Wiley, New York (1986).
12. G. Baffi, E. B. Martin and A. J. Morris, *Comput. Chem. Eng.*, **23**, 395 (1999).
13. M.-J. Park, M. T. Dokucu and F. J. Doyle III, *Ind. Eng. Chem. Res*., **43**, 7227 (2004).